Paste 2023 – GW Wilson, NA Beier, DC Sego, AB Fourie & D Reid (eds)

doi:10.36487/ACG_repo/2355_10

Numerical procedure for scaling up pressure loss from mini flow loop tests

K Kalonji *Stornoway Diamonds, Canada*

M Mbonimpa *Université du Québec en Abitibi-Témiscamingue, Canada*

T Belem *Université du Québec en Abitibi-Témiscamingue, Canada*

S Ouellet *Canadian Malartic Mine, Canada*

LP Gelinas *Agnico Eagle Mines Limited, Canada*

Abstract

Although in the literature friction factors have been developed specifically for Newtonian and non-Newtonian fluids to predict pressure loss during pipeline flow, their use for cemented paste backfills (CPB) still needs to be validated. For backfilling system feasibility studies, the flowability, pump selection and pumping requirement can be assessed through flow loop tests using full diameter (D_{full}) pipeline arrangement. At the laboratory scale, only small flow loop tests using small diameter ($D_{small} = D_{loop}$) pipeline arrangement can be conducted. However, as the pressure loss ($\Delta p/L$) is closely dependent on the pipeline inner diameter (D_i), $\Delta p/L$ measured from a small flow loop test must be correctly scaled to the field pipeline diameter ($D_{field} = D_{full}$). The objective of this paper is to present a numerical simulations-based procedure for scaling up pressure loss from small flow loop tests. For this purpose, small flow loop tests were conducted using a 27.9 m-long pipeline circuit arrangement. The small pipe's inner diameter (D_{loop}) was 0.0318 m. The pipeline circuit was instrumented with temperature probes (thermocouple) and a differential pressure meter for monitoring the evolution of the CPB temperature and pressure loss, respectively. After calibrating the non-isothermal pipe flow model in COMSOL Multiphysics® 5.2 software using temperature and pressure loss data gathered from the small flow loop tests, numerical simulations of flow loop tests were conducted to consider various filled inner diameters (D_i) of pipes from 0.05 to 0.2 m) while keeping the rheological and thermal properties of the CPB unchanged. Results indicate a negative power law relationship between the pressure loss ratio and the inner diameter ratio (D_i/D_{loop}). Work is still underway to verify if this relationship applies for different CPB mix recipes and different temperature conditions.

Keywords: *cemented paste backfill, flow loop test, scaling up, numerical simulations, pressure loss, COMSOL Multiphysics*

1 Introduction

Cemented paste backfill (CPB) is increasingly used as a tailings disposal and ground support method in underground mines to improve ore recovery (Hassani & Archibald 1998). The fresh CPB, which is considered a non-Newtonian fluid (Brackebusch 1994), is usually transported by gravity and/or pumping through a distribution network of pipes and/or boreholes from the surface to the underground stopes to be filled (Belem & Benzaazoua 2008). During the backfilling feasibility study, the flow loop test is often used to evaluate the CPB fluidity or pumpability and the pressure drops to determine the operating parameters of the distribution network: pump pressure, pipe diameter, flow rate and flow velocity (Clark et al. 1995; Cooke 2007). The flow loop test consists of pumping a fluid (CPB in this case) in a closed or looped circuit of pipes with field diameter (D_{field}) or full diameter (D_{full}). Performing a field scale test requires significant logistics (a large quantity of tailings, ready mix concrete truck, etc.) and, consequently, significant costs. However, during the backfilling feasibility study for a new mine there are usually not enough tailings available to conduct the field flow loop tests. Therefore, a laboratory scale approach with reasonable quantities of tailings and a mini

flow loop circuit with small inner diameter pipes ($D_{i\text{-}small}$) is a solution to consider. It should be noted, however, that the pressure drops (Δp) are highly dependent on the pipe inner diameter (Cooke & Lazarust 1993). In addition, the pressure losses measured during the flow loop test using a small flow loop system must be scaled to the actual diameter of the pipes installed in the field. The scaling procedure is based on a dimensional analysis using the Vaschy-Buckingham theorem. This theorem states that if a physical problem is described by *N* variables and parameters in *r* dimensions or *r* independent variables, then it is possible to describe an implicit dimensionless function (Deville 2022).

The objective of this paper is to present a procedure for scaling up the pressure losses generated during a flow loop test using a small flow loop circuit, based on numerical simulations of the CPB flow.

2 Theory

The pressure gradient ($\Delta p/L$) generated by a flowing Newtonian or non-Newtonian fluid in a circular pipe is calculated using the Darcy-Weisbach equation (Swamee & Aggarwal 2011):

$$\frac{\Delta p}{L} = f \frac{\rho\, U^2}{2\, D} \tag{1}$$

where:

- U = flow velocity (m/s).
- f = Darcy friction factor (–).
- ρ = fluid density (kg/m^3).
- D = hydraulic diameter of pipe (m).
- L = pipe length (m).

The friction factor f in Equation 1 can be calculated using the following relationship (Assefa & Kaushal 2015):

$$f = \left(f_{lam}^{b} + f_{turb}^{b}\right)^{1/b} \tag{2}$$

The parameter *b* is given by the following relationship:

$$b = 1.7 + \frac{40{,}000}{Re} \tag{3}$$

where Re is Reynolds number (–).

The parameters f_{lam} and f_{turb} represent the friction coefficients for laminar and turbulent fluid flow, respectively (Assefa & Kaushal 2015; Swamee & Aggarwal 2011). The parameters f_{lam} and f_{turb} also depend on the type of fluid (Newtonian or non-Newtonian). A Newtonian fluid is governed by the Newtonian fluid law (Barnes et al. 1989; Mezger 2006):

$$\eta = \frac{\tau}{\dot{\gamma}} \tag{4}$$

where:

- η = dynamic viscosity of Newtonian fluid (Pa.s).
- τ = shear stress (Pa).
- $\dot{\gamma}$ = shear rate (1/s).

A non-Newtonian Bingham fluid is described by the following relation:

$$\tau = \tau_B + \eta_B \dot{\gamma} \tag{5}$$

where:

τ_B = Bingham yield stress (Pa).

η_B = Bingham plastic viscosity (Pa.s).

Table 1 summarises the formulas used to calculate the parameters f_{lam} et f_{turb} (Farshad et al. 2001; Taylor et al. 2006).

Depending on the heat exchange, the increase in fluid temperature during pipeline transport is attributed to heat-related viscous dissipation between fluid layers and internal friction between the fluid and the wall (Winter 1987). The heat-related viscous dissipation depends on the type of fluid (Newtonian or non-Newtonian), the consistency of the fluid, the type of flow and the pipe size (Winter 1987).

Table 1 Darcy friction factor formulas for Newtonian and non-Newtonian Bingham fluids

Flow regime	Newtonian fluid	Non-Newtonian Bingham fluid
Laminar	$f = \frac{64}{Re}$ With $Re = \frac{\rho DU}{\eta}$	$f_{lam} = \frac{64}{Re} + \frac{10.67 + 0.1414(He/Re)^{1.143}}{[1 + 0.0149(He/Re)^{1.16}]Re}\left(\frac{He}{Re}\right)$ where $Re = \frac{\rho DU}{\eta_B}$; and $He = \frac{\rho D^2 \tau_B}{{\eta_B}^2}$ He = Hedström number (-)
Turbulent	$\frac{1}{\sqrt{f}} = -2\ \log\left[\frac{2.51}{Re\sqrt{f}} + \frac{\varepsilon}{3.71D}\right]$ With $0 \leq \varepsilon/D \leq 0.05$ ε = absolute surface roughness (m)	$f_{turb} = 4.10^{a_o} \times Re^{-0.193}$ with $a_o = -1.47\left[1 - 0.146\ e^{(-2.9\ 10^{-5} He)}\right]$ Re and He numbers for laminar flow are valid for turbulent flow

Cooke et al. (1992) observed an increase in the temperature of a CPB mixture during flow loop tests. For this reason, flow loop tests of cementitious materials (such as CPB, concrete, cement paste) are often equipped with heat exchange systems to maintain the constant temperature of the fluid during the test (Cooke et al. 1992). However, there is a variation in CPB temperature related to viscous dissipation and heat exchange with the external environment during the CPB flow in the full-scale pipe (i.e. Creber et al. 2017). This induces non-isothermal conditions of CPB transport in the pipe. Thus the generalised energy equation of a fluid flowing in a cylindrical pipe is given by the following relationship (COMSOL 2012):

$$\rho\ A\ C_p \frac{\partial T}{\partial t} + \rho A C_p U \nabla T = \nabla(A\lambda\nabla T) + \frac{1}{2} f \frac{\rho A}{D} |U|^3 + Q + Q_w \quad (6)$$

where:

A = the cross-sectional area of the pipe.

λ = the thermal conductivity.

Cp (J/kg°C) = the specific or mass heat capacity.

T (°C) = the temperature.

Q (W/m) = the heat source flux (heat related to hydration, for example).

Qw (W/m) = the heat flux at the wall.

The heat flux at the wall (Q_w) is given by the following relationship (COMSOL 2012):

$$Q_w = h_{loc}(x)\,\pi\,D\,\left(T_w(x) - T_f(x)\right) \tag{7}$$

where:

T_w = wall temperature.

T_f = the fluid temperature.

h_{loc} = the heat transfer coefficient given by the following relationship (Bird et al. 2002; Wagner 2010):

$$h_{loc} = \frac{Nu\,\lambda}{D} \tag{8}$$

where Nu is the Nusselt number.

This number reflects the ratio of heat quantities transported by convection and conduction. An internal forced turbulent convective flow of a Newtonian fluid is given by (Incropera et al. 2007):

$$Nu = \frac{(f/8)(Re-1000)Pr}{1+12.7(f/8)^{1/2}\left(Pr^{2/3}-1\right)} \tag{9}$$

where Pr is the Prandtl number (see Equation 10) given by the following relationship:

$$Pr = \frac{C_p\eta}{\lambda} \tag{10}$$

For a non-Newtonian fluid (e.g. Bingham) flowing in a cylindrical pipe, the internal Nusselt number Nu can be determined from data providing the variation of the Nusselt number Nu with the dimensionless number Ψ for the Herschel–Bulkley and Bingham fluids, according to Cruz et al. (2012) and Alves et al. (2015).

Similarly, if a forced external convection related to airflow at a given velocity U_{air} and temperature T_{air} around the circular duct is considered, the Nusselt number Nu_{ext} can be calculated using the following expression (Incropera et al. 2007; Ferrouillat et al. 2011):

$$Nu_{ext} = 0{,}3 + \frac{0{,}62\sqrt{Re}Pr^{1/3}}{\left[1+(0{,}4/Pr)^{2/3}\right]^{1/4}}\left[1 + (Re/282\times10^3)^{5/8}\right]^{4/5} \tag{11}$$

However, Equation 11 is recommended for $Re \times Pr$ >0.2 (Incropera et al. 2007).

3 Experimental program

The experimental program is subdivided into three main stages:

- Physical and mineralogical characterisations of the raw mine tailings X and Y.
- Rheological and thermal characterisations of uncemented paste tailings (PT) and CPB to determine the effect of cement addition.
- PT and CPB flow loop tests using a small flow loop circuit.

3.1 Physical and mineralogical characterisations of the mine tailings and backfill mixtures preparation

The Malvern Mastersizer 3000 laser granulometer was used to determine the particle size distribution (PSD) of the tailings. The specific gravity (G_S) of the tailings grains was measured using the Micromeritics AccuPyc 1330 helium pycnometer. The mineral phases of the tailings were identified using X-ray diffraction.

Figure 1 presents the PSD curves of mine tailings X and Y. Tailings sample X is relatively coarser than tailings Y sample. Table 2 lists the physical and mineralogical characteristics of the mine tailings X and Y used. In this table, D_x, C_U, C_C and P_y represent, respectively, the diameter corresponding to x% passing on the sieve, the uniformity coefficient, the curvature coefficient and the % passing on the y (µm) sieve. Following the Unified Soil Classification System (USCS), the mine tailings X and Y are low plastic silts (ML). The G_S of these X and Y tailings are 2.74 and 2.93, respectively. In terms of mineralogy, albite (53.5%), quartz (23.6%), chlorite (11.2%) and calcite (8.1%) are the major mineral phases in tailings sample X. Major mineral phases of the tailings sample Y were quartz (40.3%), albite (19.5%), muscovite (14.6%), ankerite (8.8%) and chlorite (8.1%).

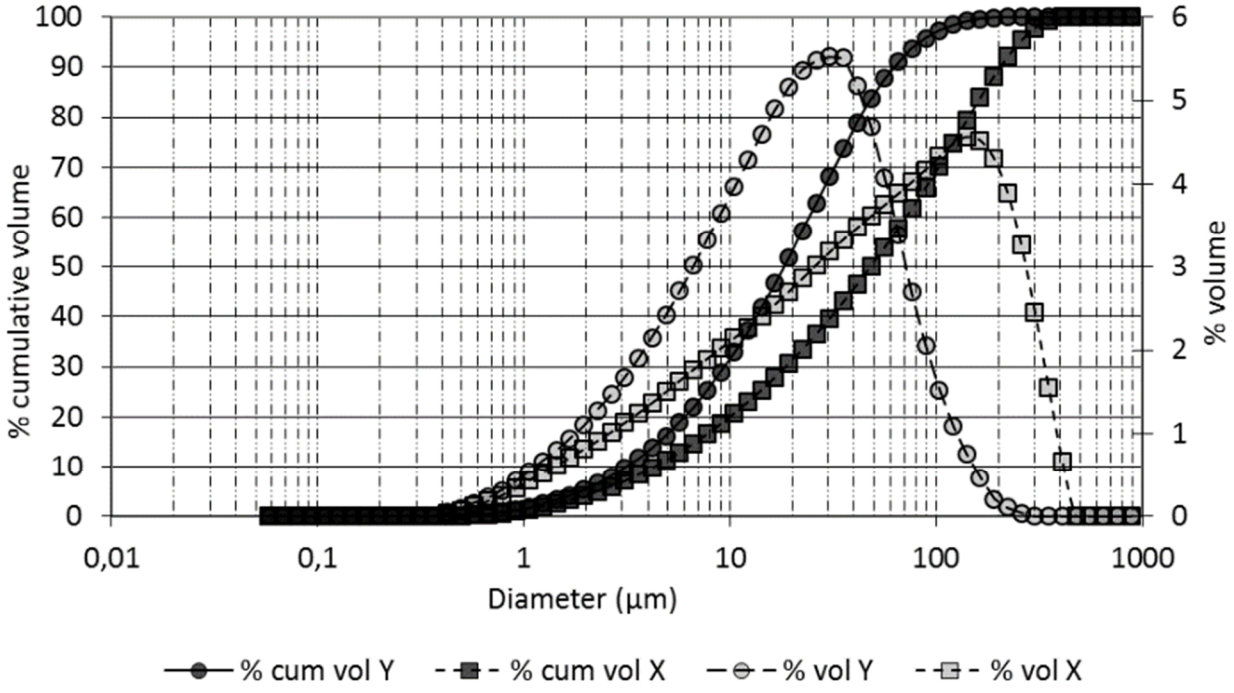

Figure 1 Particle size distribution of the mine tailings X and Y

Table 2 Physical and mineralogical properties of the mine tailings X and Y

Parameter	Units	Values	
		Tailings X	Tailings Y
Specific gravity (G_S)	–	2.74	2.93
D_{10}	µm	4.3	3.1
D_{30}	µm	18.6	9.4
D_{50}	µm	48	18.3
D_{60}	µm	71.5	24.4
D_{90}	µm	205.6	62.6
$C_C = D_{30}^2/(D_{60}\ D_{10})$	–	1.1	1.2
$C_U = (D_{60}/D_{10})$	–	16.6	7.7
$P_{2µm}$	%	4.1	5.4
$P_{20µm}$	%	31	53
$P_{80µm}$	%	64	94
Mineral phases	**Units**	**Values**	
Albite	%	53.5	19.5
Quartz	%	23.6	40.3
Chlorite	%	11.2	8.1
Calcite	%	8.1	2.4
Actinolite	%	2.1	0
Gypsum	%	1	0
Muscovite	%	0.4	14.6
Pyrite	%	0	0.4
Ankerite	%	0	8.8
Microline	%	0	1.3
Magnetite	%	0	4.6
Total		**100**	**100**

PT and CPB are the two types of mixture used in the flow loop testing. The PT mixtures were prepared with tap water and tailings from the samples X and Y at a dry solid mass concentration C_w of 74 and 71%wt, respectively. These mixtures are called PT-X and PT-Y in the following. The CPB mixture was prepared at a dry solid mass concentration C_w of 71%wt with tap water, tailings from the mine Y and high early Portland cement (Type HE, or Type III according to ASTM C 150-07) at a cement-to-dry tailings ratio (B_w) of 5%wt. This mixtures is called CPB-Y hereafter. This type of cement is typically used when high short-time strength is required. A preliminary flow loop test using only tap water was performed for validating the test results.

Progressive mixing of the water and tailings (and binder) was carried out using a pump mixer (see Figure 2) until achieving a standard Abrams's cone slump of approximately 10 inches or 254 mm (Figure 3) according to ASTM C143/C 143 M-05. Approximately 10 inches of cone slump corresponds to the dry solid mass concentration C_w of 74 and 71% for PT and CPB, respectively. This slump value corresponds to a fluidity or

yield stress that must be overcome for flow through the circuit to occur without blockage and according to the specifications of the pump mixer used. This test is also used to assess the pumpability, or workability, of the CPB.

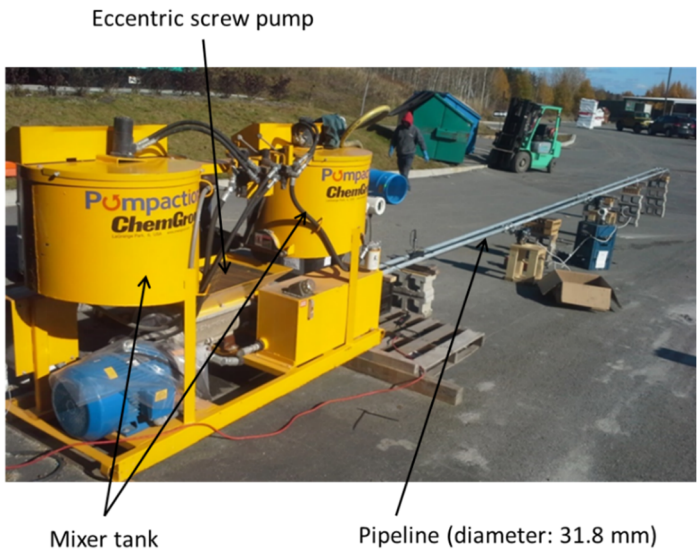

Figure 2 Small flow loop testing circuit: image of the circuit layout

Figure 3 Standard slump test using Abrams's cone on the paste tailings sample X

3.2 Rheological and thermal characterisation of PT and CPB mixtures

The rheological characterisation of the PT and CPB mixtures was performed using an AR2000 rheometer (TA Instruments) equipped with a vane geometry and a cylindrical Peltier system to control the sample temperature during the test. The continuous ramp flow procedure and control shear rate mode in steady state flow regime was used. The material was first pre-sheared (to de-structure the material) at a constant shear rate of 100 s^{-1} for 90 seconds, then allowed to stand for 15 seconds and, finally, subjected to decreasing shear rate steps from 100 to 0 s^{-1} for 70 seconds. Even if thixotropy can be observed for PT and CPB, it should be mentioned that rheological properties determined on the flow and viscosity curves obtained in descending mode are suitable for the design of the flow in CPB pipelines (Pullum 2007).

Figure 4 shows the average rheograms of the PT and CPB mixtures. It can be observed that the rheograms of PT-X, PT-Y and CPB-Y are linear. Thus the Bingham flow model can better describe the rheological behaviour of PT-X, PT-Y and CPB-Y with a relative error of 6.91, 5.43 and 2.82‰, respectively. From the fitting linear equations, the shear yield stress (τ_o) values are 33.8, 30.2 and 36.4 Pa for PT-X, PT-Y and CPB-Y, respectively. In addition, the Bingham plastic viscosity (η_B) values are 0.51, 0.63 and 0.74 Pa.s for PT-X, PT-Y and CPB-Y, respectively.

The thermal properties measurement of PT and CPB mixtures was then performed using the SH-1 thermal probe of the KD2-Pro thermal analyser. For this purpose, the fresh PT and CPB mixtures were filled into a plastic mould (height = 10.2 cm, diameter = 5.1 cm). Upon completion of filling the moulds with the fresh PT and CPB mixtures, immediate measurements of the thermal properties were performed.

PT samples PT-X, PT-Y and CPB-Y have thermal conductivities (λ) of 1.56, 1.68 and 1.68 W/m°K, respectively, and specific heat capacities (C_p) of 1,535, 1,377 and 1,380 J/kg°K, respectively.

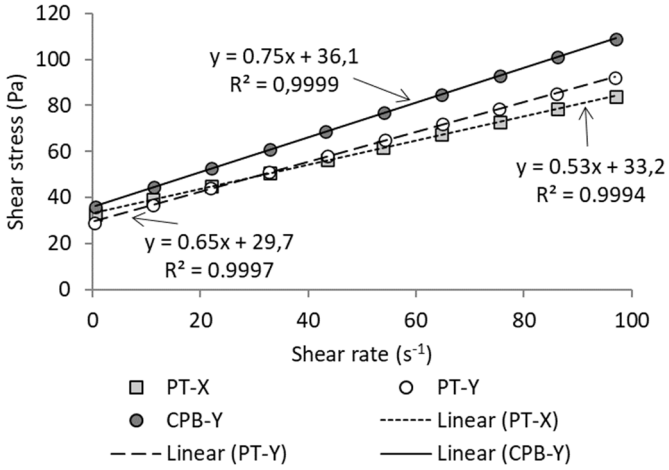

Figure 4 Rheograms of PT-X, PT-Y and CPB-Y used for small flow loop testing

3.3 Flow loop tests

Figure 5 shows the small flow loop circuit used to perform the flow loop tests. This circuit is mainly composed of an eccentric screw pump mixer with a nominal capacity of 1,800 kPa (18 bar) and a 27.9 m-long circular (steel) loop pipe. The inner diameter of the piping is 31.8 mm. The pump has a maximum pumping capacity of 76 L/s. This pump is equipped with two mixing tanks with a total capacity of 265 L and a hopper of 57 L.

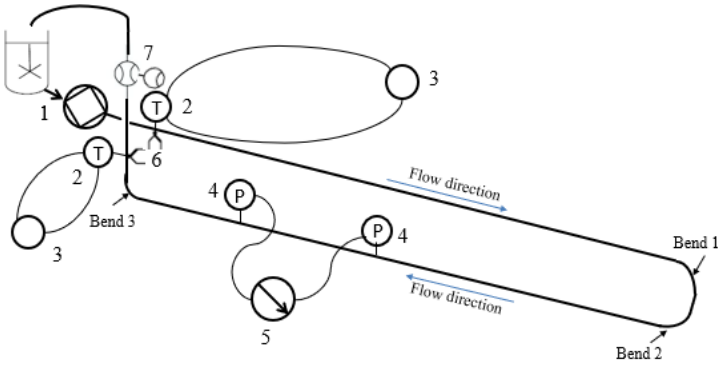

Figure 5 Schematic diagram of the flow loop testing circuit layout: (1) mixer pump; (2) temperature probes; (3) multimeters; (4) pressure sensors; (5) differential pressure transmitter; (6) thermocouples type K; (7) electromagnetic flowmeter

The small flow loop circuit was instrumented with two Intempco RTD model R24 temperature probes (one at the inlet and the other at the outlet) with an accuracy of ±0.1°C, two pressure sensors 3 m apart, located at 5.7 and 8.7 m downstream from bend 2 (or 6 and 3 m upstream from bend 3), respectively, and connected to a differential pressure transmitter, a Process Master FEP315 electromagnetic flowmeter and two type K thermocouples installed on the surface of the pipe (the first at the inlet pipe circuit and the second at the outlet pipe circuit) (see Figure 5). Each flow loop test was conducted for 60 minutes. Data were recorded at 5, 10, 15, 20, 30, 45 and 60 minutes.

4 Numerical calibrations of the small flow loop tests

The non-isothermal pipe flow numerical model (in 3D stationary mode) of COMSOL Multiphysics® 5.2 was used to calibrate the flow and heat transfer in the small flow loop circuit. The non-isothermal pipe flow model is a module of the fluid flow interface. It is a coupling of the physical pipe flow and heat transfer in pipe models, which allows one to determine the hydrodynamic (pressure, flow velocity) and heat transfer (change in fluid temperature, wall heat flux) parameters considering the heat generated by viscous dissipation and internal friction generated by fluid flow in the pipe. The physical pipe flow model involves analytical equations presented in Table 1.

Table 3 summarises the input parameters used for the numerical simulations. These parameters are mainly the rheological and thermal properties of the fluids, the circuit characteristics (diameter, thermal properties of the pipe), the thermal conditions (initial temperature of the fluid, external temperature) and the hydrodynamic parameters (fluid flow velocity and outlet pressure). The thermal properties (thermal conductivity and thermal capacity) were considered constant as it was observed by Beya et al. (2015) that the PT and CPB mixtures were not affected by the temperature variation between 2 and 40°C (Beya et al. 2015).

Table 3 Inlet parameters used for numerical simulations of the small flow loop tests

Input parameters	Water	PT-X	PT-Y	CPB-Y
Fluid density, ρ (kg/m^3)	1,000	1,885	1,877	1,880
Solid mass concentration, C_w (%)	–	74	71	71
Bingham yield stress, τ_o (Pa)	–	33.8	30.2	36.4
Bingham plastic viscosity, η (Pa.s)	0.001	0.509	0.633	0.744
Thermal conductivity, λ (W/mK)	0.60	1.56	1.68	1.68
Specific heat capacity of fluid, C_p (J/kgK)	4.182	1.535	1.377	1.380
Inlet temperature of fluid, T_f (°C)	9.7	17.6	22.5	26.7
Flow velocity of fluid, U (m/s)	1.38	1.42	1.37	1.31
Pipe inner diameter, D or D_i (m)	0.03175	0.03175	0.03175	0.03175
Pipe thermal conductivity, λ_{wall} (W/mK)	45	45	45	45
Pipe wall thickness, e (m)	0.003	0.003	0.003	0.003
External temperature, T_{air} (°C)	2	2	12	14
Air velocity, U_{air} (m/s)	0.01	0.3	0.3	0.9
External Nusselt, Nu_{ext}	*	14	13.4	23
Internal Nusselt, Nu	*	4.65	4.65	4.65

5 Results and discussion

5.1 Flow loop test results

The Figures 6a, b, c and d present the variation of flow velocity (U) and pressure gradient ($\Delta p/L$) in the circuit as a function of test time, respectively, for water, PT-X, PT-Y and CPB-Y. It can be noted that the water U fluctuates between 1.33 and 1.37 m/s in the first 10 minutes of the flow test before stabilising at around 1.39 m/s. In response, the pressure gradient ($\Delta p/L$) augments with increasing velocity over time before reaching a steady state with $\Delta p/L \approx$ 0.60 kPa/m.

For PT-X, the flow U varies from 1.37 to 1.41 m/s in the first 15 minutes before stabilising at around 1.42 m/s. The pressure gradient varies from to 27.4 to 25.1 kPa/m for almost constant flow velocities from 10 minutes onwards. There is a decrease in the pressure gradient ($\Delta p/L$) with increasing PT-X temperature. This is probably related to the decrease in the rheological properties of PT-X with increasing temperature. Indeed, Kalonji et al. (2015) observed that the rheological properties of PT mixtures decreased with increasing temperature. The shear yield stress and the Bingham plastic viscosity of PT tend to decrease with the increase of temperature.

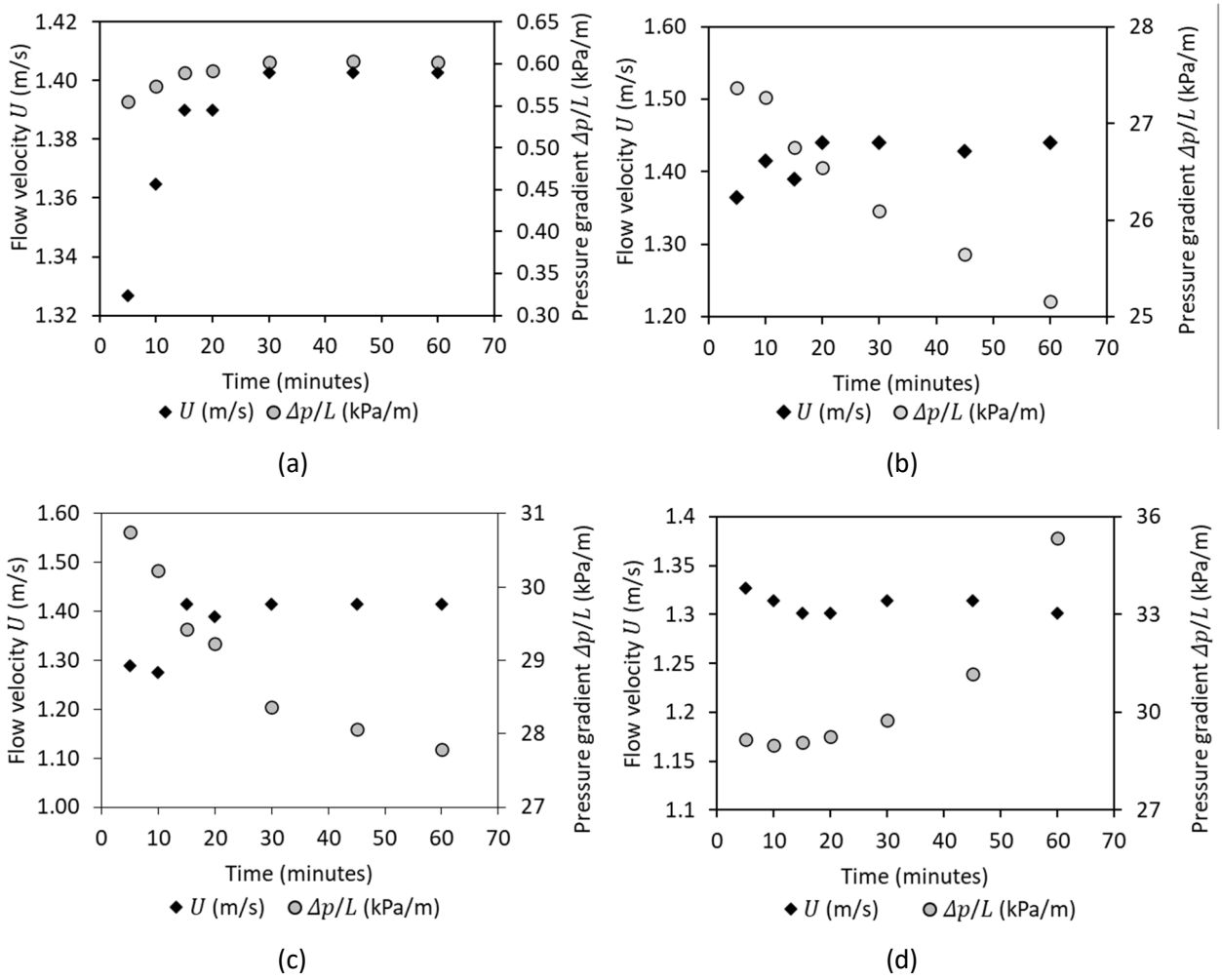

Figure 6 Variation in flow velocity (U) and pressure drop ($\Delta p/L$) as a function of flow time during small flow loop tests for: (a) water; (b) PT-X; (c) PT-Y; and (d) CPB-Y

For PT-Y, the pressure gradient ($\Delta p/L$) decreases (from 30.7 to 27.3 kPa/m) with recirculation time and because of the increase in temperature, although the flow velocity (U) remained almost constant after 10 minutes. (Figure 6c). This can be explained by the same reasons given for PT-X: namely, a decrease in the rheological properties with increasing temperature.

For the CPB-Y (with yield stress = 36.4 Pa and Bingham plastic viscosity = 0.74 Pa.s), the flow velocity (U) remained almost constant during the test at around 1.3 m/s (Figure 6d). Note that the linear pressure gradient ($\Delta p/L$) remained almost constant at around 29 kPa/m during the first 20 minutes before increasing and reaching 35 kPa/m at the 60 minute mark (Figure 6d).

Notice on Figure 6d a trend of pressure gradient ($\Delta p/L$) increase with flow time and CPB-Y temperature increase. This increase of pressure gradient ($\Delta p/L$) is likely due to the increase in rheological properties with rising temperature and possibly the cement hydration process. Indeed, the rheological properties tend to increase with rising temperature for CPB mixtures using hydraulic cements (Wu et al. 2013; Kalonji et al. 2015).

5.2 Calibration results

Here only measured and calculated pressure drops are compared, without presenting a comparison of temperatures measured by the probes installed on the circuit (see Figure 5) and calculated values. For flow loop testing with water, the water flow velocity (U) was at a value of 1.33 m/s for a pressure gradient of 0.55 kPa/m after five minutes of flow (see Figure 6a). A numerical simulation performed considering this velocity gives the pressure distribution shown in Figure 7a. A pressure of 119 kPa is required to circulate water in the small circuit at a constant velocity of 1.33 m/s, with an Re of 31,549 and a friction coefficient f of 0.02. In this case, the simulated pressure gradient ($\Delta p/L_{sim}$) is 0.64 kPa/m. This value is close to the experimental pressure gradient value of water ($\Delta p/L_{exp}$ = 0.55 kPa/m).

Figure 6b presents the results of the PT-X flow loop test. The flow velocity of PT-X was 1.36 m/s after five minutes of flow. A numerical simulation performed considering this velocity gives the pressure distribution presented in Figure 7b for the flow cycle (at five minutes). In this case, a pressure of approximately 873 kPa is required to flow the PT-X at a velocity of 1.36 m/s, with a Re of 160, a He of 248 and a friction coefficient f of 0.5. The simulated pressure gradient ($\Delta p/L_{sim}$) of the PT-X mixture is 27.7 kPa/m using these calculated figures. This value is moderately higher than the experimental value ($\Delta p/L_{exp}$ = 27 kPa/m).

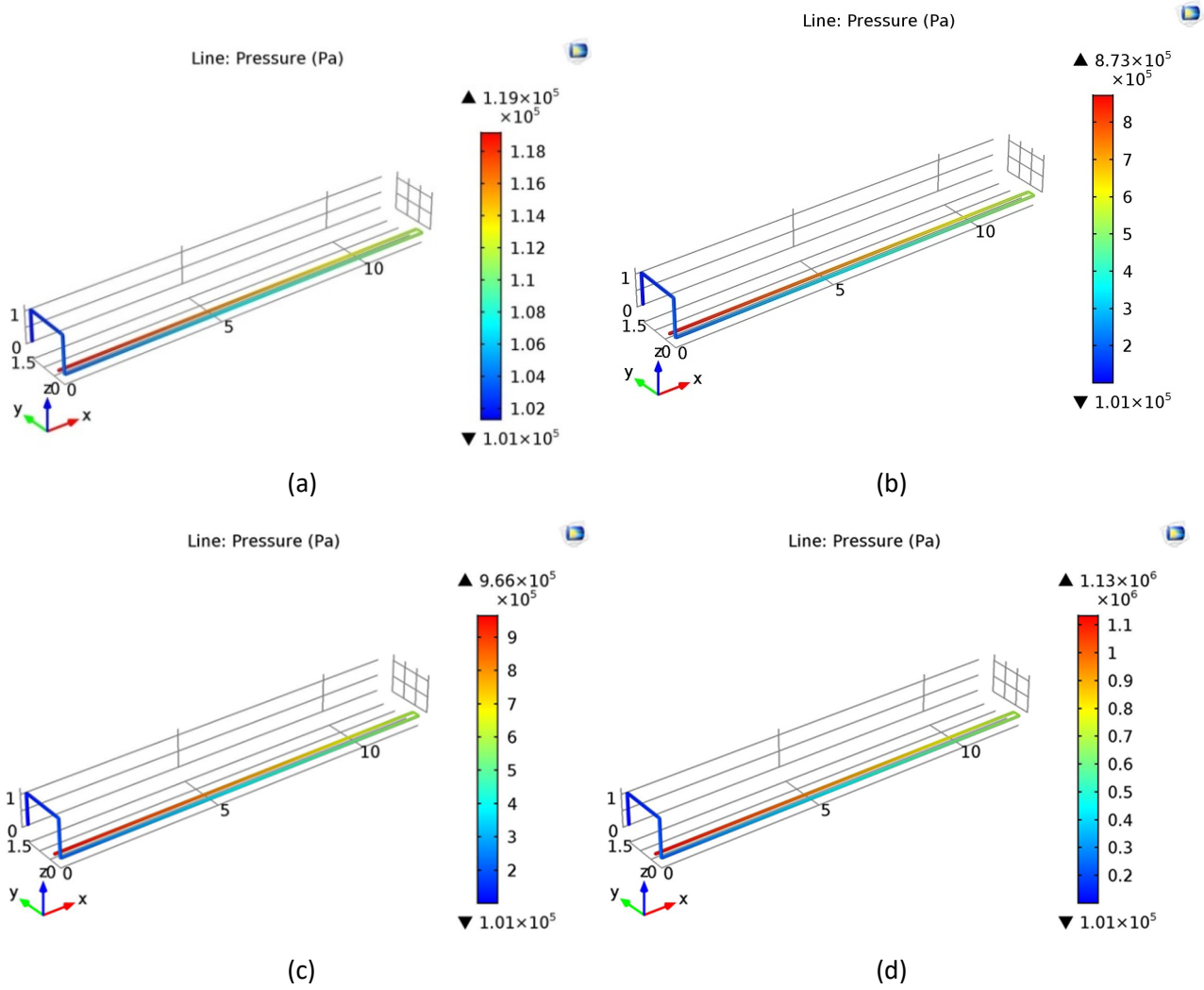

Figure 7 Numerical simulated pressure distribution for five-minute flow loop tests using COMSOL: (a) water; (b) PT-X; (c) PT-Y; and (d) CPB-Y

Figure 6c presents the PT-Y flow loop test results. The flow velocity of PT-Y was 1.29 m/s after five minutes of flow. A numerical simulation performed considering this velocity gives the pressure distribution presented

in Figure 7c for the flow cycle (at five minutes). In this case, a pressure p of approximately 966 kPa is required to pump PT-Y through the small loop test circuit at a velocity of 1.29 m/s, with a Re of 122, a He of 143, and a friction coefficient f of 0.63. Thus, the simulated pressure gradient for PT-Y ($\Delta p/L_{sim}$) is 31 kPa/m. This is almost identical to the value of the pressure gradient obtained experimentally ($\Delta p/L_{exp}$ = 30.7 kPa/m).

For CPB-Y, the average velocity of 1.31 m/s is equal to the velocity reached after five minutes of flow. In this case, a single numerical simulation was performed to evaluate the pressure gradient at five minutes. A pumping pressure p of approximately 1,135 kPa is required to pump CPB-Y through the small flow loop test circuit at a velocity of 1.31 m/s (Figure 7d), with a Re of 105, a He of 125 and a friction coefficient f of 0.73. Therefore, the simulated linear pressure gradient ($\Delta p/L_{sim}$) of CPB-Y is approximately 37 kPa/m. Note that the latter is significantly higher than that obtained experimentally ($\Delta p/L_{exp}$ = 29.2 kPa/m) in the small flow loop test for CPB-Y. The discrepancy between the two pressure gradient values can probably be related to the formation of the lubrication layer in the pipe during the flow loop test because of the cement addition (Cooke et al. 1992). This may result in a discrepancy between the rheological behaviour recorded in the laboratory and that recorded in the pipe. Furthermore, this discrepancy may be explained by poor rheometry of concentrated suspension that is an exacting task.

5.3 Scale-up

The small flow loop test circuit used to perform the flow loop tests use a D_{loop} diameter of 0.03175 m. Nevertheless, the CPB pipeline distribution diameters are generally larger (between 0.1 and 0.2 m). Since pressure gradients are influenced by diameter, it is necessary to establish a relationship between the pressure gradient ($\Delta p/L_{loop}$) obtained using the D_{loop} diameter of 0.03175 m and that ($\Delta p/L_i$) obtainable at a diameter D_i (m) of the targeted distribution system. Thus numerical simulations of the PT-X, PT-Y and CPB-Y flow loop tests for four different diameters D_i (0.05 m, 0.1 m, 0.15 m and 0.2 m) were used to calculate the corresponding different pressure gradient ($\Delta p/L_i$). Table 4 presents the different simulated ($\Delta p/L_i$) values.

Table 4 Simulated pressure gradient $\Delta p/L_i$ at different internal diameter for PT-X, PT-Y and CPB-Y

	D (m)	$\Delta p/L_i$ (kPa/m)		
		PT-X	PT-Y	CPB-Y
Small diameter	0.03175	27.7	31.0	37.0
Full-scale diameter	0.05	12.4	13.7	16.3
	0.1	4.0	4.2	5.0
	0.15	2.2	2.2	2.7
	0.2	1.4	1.4	1.7

Figure 8a presents the variation of the pressure gradient ratio $(\Delta p/L_i)/(\Delta p/L_{loop})$ as a function of the pipe diameter ratio (D_i/D_{loop}) for PT-X, PT-Y and CPB-Y mixtures. This highlights that the type of mixture does not affect the ratios, and hence demonstrates the relationship between the pipe diameter ratio and pressure gradient ratio (Figure 8a). Figure 8b presents the established relationship between the pressure gradient ratio and the pipe diameter ratio which is given as follows (valid for the small circuit used for small flow loop tests):

$$(\Delta p/L_i)/(\Delta p/L_{loop}) = 0.9631(D_i/D_{loop})^{-1.648} \quad (12a)$$

$$(\Delta p/L_i) = 0.9631(\Delta p/L_{loop})(D_i/D_{loop})^{-1.648} \quad (12b)$$

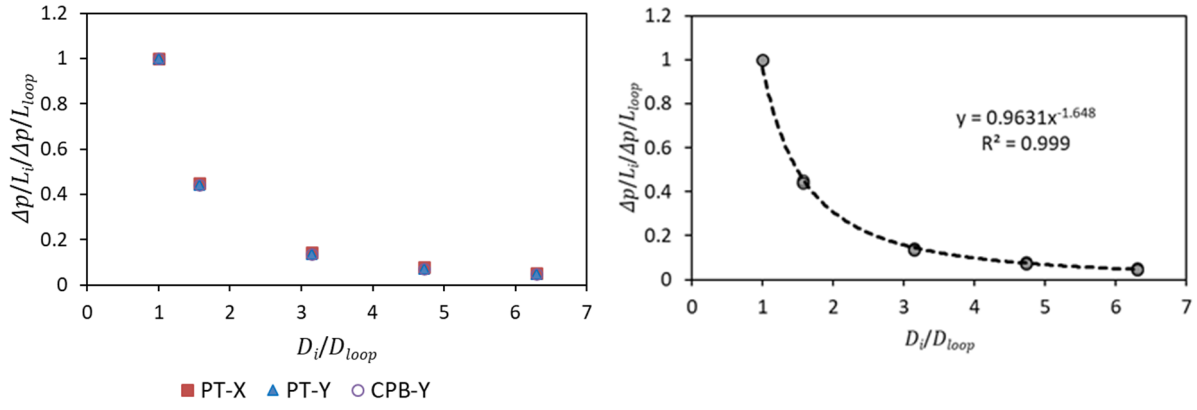

(a) (b)

Figure 8 Pressure gradient scaling up: (a) pressure gradient ratio versus pipe inner diameter ratio for PT-X, and PT-Y and CPB-Y; and (b) scaling relationship of flow loop test results using a small loop flow circuit

When designing the backfill system with a given backfill flow rate, relation 12b allows prediction of the pressure gradient for different internal pipe diameter ratios based on the flow test data in a mini loop circuit and, therefore, selection of the appropriate pipe diameter.

6 Conclusion

The objective of this paper was to establish a scaling relationship for the flow loop test in a small circuit for full-scale applications. Dimensional analysis based on experimental test data and numerical simulations using COMSOL of the fluid flow for the full diameter flow circuit resulted in a relationship that can be used. This relationship is valid specifically for the small circuit configuration used in this study for the flow loop tests. It can be noted that the established relationship is independent of the type of fluid. However, the applicability of the established relationship is subject to an extensive analysis over a wide range of materials and behaviours likely to be encountered in operations.

Acknowledgment

The authors would like to acknowledge the Fonds de recherche du Québec, Nature et technologies, Agnico Eagle Mines Ltd., the Research Institute of Mines and Environment, and the Natural Sciences and Engineering Research Council of Canada for their financial support.

References

Alves, MA, Baptista, A & Coelho, PM 2015, 'Simplified method for estimating heat transfer coefficients: constant wall temperature case', *Heat and Mass Transfer*, vol. 51, pp. 1041–104

Assefa, KM & Kaushal, DR 2015, 'A comparative study of friction factor correlations for high concentrate slurry flow in smooth pipes', *Journal of Hydrology and Hydromechanics*, vol. 63, pp. 13–20, https://doi.org/10.1515/johh-2015-0008

Barnes, HA, Hutton, JF & Walters, K 1989, *An Introduction to Rheology*, Elsevier Science Publishers, Amsterdam.

Belem, T & Benzaazoua, M 2008, 'Design and application of underground mine paste backfill technology', *Geotechnical and Geological Engineering*, vol. 26, pp. 147–174, http://dx.doi.org/10.1007/s10706-007-9154-3

Beya, FK, Mbonimpa, M, Belem, T, Benzaazoua, M, Kalonji, K & Ouellet, S 2015, 'Preliminary study of the influence of temperature and salinity on the thermal properties of hardening cemented paste backfill', *Proccedings of the 68th Canadian Geotechnical Conference, GeoQuebec 2015: Challenges from North to South*, Québec, Canada, 20–23 September 2015.

Bird, RB, Stewart,WE & Lightfoot, EN 2002, *Transport Phenomena*, 2nd edn, John Wiley & Sons, Inc. New York.

Brackebusch, FW 1994, 'Basics of paste backfill systems', *Minerals Engineering,* vol. 46, pp. 1175–1178, https://doi.org/10.1016/0148-9062(95)90153-v

Clark, CC, Vickery, JD & Backer, RR 1995, *Transport of Total Tailings Paste Backfill: Results of Full-Scale Pipe Test Loop*, *Report of Investigation, RI 9573*, United States Buraeu of Mines, 37 p.

COMSOL 2012, *COMSOL Multiphysics Reference Manual*, COMSOL, Burlington, p. 750.

Cooke, R 2007, 'Backfill pipeline distribution systems – design methodology review', in F Hassani & J Archibald (eds), *Proceedings of the 9th International Symposium on Mining with Backfill*, Canadian Institute of Mining, Metallurgy and Petroleum, Westmount.

Cooke, R & Lazarus, JH 1993, 'Hydraulic transport systems for the backfilling of deep mines', *Journal of the European Ceramic Society*, vol. 93, pp. 25–30.

Cooke, R, Spearing, A & Gericke D 1992, 'The influence of binder addition on the hydraulic transport of classified-tailings backfill', in *Journal of the Southern African Institute of Mining and Metallurgy*, vol. 92, pp. 325–329.

Creber, KJ, McGuinness, M, Kermani, MF & Hassani, FP 2017, 'Investigation into changes in pastefill properties during pipeline transport', *International Journal of Mineral Processing*, vol. 163, pp. 35-44.

Cruz, DA, Coelho, PM & Alves, MA 2012, 'A simplified method for calculating heat transfer coefficients and friction factors in laminar pipe flow of non-Newtonian fluids', *ASME: Journal of Heat Transfer*, vol. 134, https://doi.org/10.1115/1.4006288

Deville, MO 2022, *An Introduction to the Mechanics of Incompressible Fluids*, Springer, https://doi.org/10.1007/978-3-031-04683-4

Farshad, F, Rieke, H & Garber, J 2001, 'New developments in surface roughness measurements, characterization and modeling fluid flow in pipe', *Journal of Petroleum Science and Engineering*, vol. 29, pp. 139–150, http://dx.doi.org/10.1016/S0920-4105(01)00096-1

Ferrouillat, S, Bontemps, A, Ribeiro, JP, Gruss, JA & Soriano, O 2011, 'Hydraulic and heat transfer study of SiO2/water nanofluids in horizontal tubes with imposed wall temperature boundary conditions', *International Journal of Heat and Fluid Flow*, vol. 32, pp. 424–439, https://doi.org/10.1016/j.ijheatfluidflow.2011.01.003

Hassani, F & Archibald, JF 1998, *Mine Backfill*, Canadian Institute of Mining, Metallurgy and Petroleum, Montreal.

Incropera, FP, Dewitt, DP, Bergman, TL & Lavine, AS 2007, *Fundamentals of Heat and Mass transfer*, 6th edn, John Wiley & Sons, Hoboken.

Kalonji, K, Mbonimpa, M, Belem, T, Benzaazoua, M, Beya, F & Ouellet, S 2015, 'Preliminary investigation of the effect of temperature and salinity on the rheological properties of fresh cemented paste backfills', *Proceedings of the 68th Canadian Geotechnical Conference, GeoQuebec 2015: Challenges from North to South*, Québec, Canada, 20-23 September 2015.

Mezger, TG 2006, *The Rheology Handbook for Users of Rotational and Oscillatory Rheometers*, Vincentz Network GmbH & Co. KG, Hannover.

Pullum, L 2007, 'Pipelining tailings, pastes and backfill', in R Jewell & AB Fourie (eds), *Paste 2007: Proceedings of the Tenth International Seminar on Paste and Thickened Tailings*, Australian Centre for Geomechanics, Perth, pp. 113–127.

Swamee, PK & Aggarwal, N 2011, 'Explicit equations for laminar flow of herschel-bulkley fluids', *Canadian Journal of Chemical Engineering,* vol. 89, pp. 1426–1433, https://doi.org/10.1002/cjce.20484

Taylor, JB, Carrano, AL & Kandlikar, SG 2006, 'Characterization of the effect of surface roughness and texture on fluid flow—past, present, and future', *International Journal of Thermal Sciences*, vol. 45, p. 962–968.

Wagner, W 2010, 'Heat transfer to non-Newtonian fluids', in P Stephan, S Kabelac, M Kind, H Martin, D Mewes & K Schaber (eds), *VDI Heat Atlas*, 2nd edn, Springer-Verlag, Berlin.

Winter, HH 1987, 'Viscous dissipation term in energy equations', *American Institute of Chemical Engineers,* vol. 7, pp. 27–34.

Wu, D, Fall, M & Cai SJ 2013, 'Coupling temperature, cement hydration and rheological behaviour of fresh cemented paste backfill', *Minerals Engineering*, vol. 42, pp. 76–87, https://doi.org/10.1016/j.mineng.2012.11.011